

IS THE POST-AGB STAR SAO 40039 MILDLY HYDROGEN-DEFICIENT?

S. Sumangala Rao², Gajendra Pandey², David L. Lambert³

and

Sunetra Giridhar²

ABSTRACT

We have conducted an LTE abundance analysis for SAO 40039, a warm post-AGB star whose spectrum is known to show surprisingly strong He I lines for its effective temperature and has been suspected of being H-deficient and He-rich. High-resolution optical spectra are analyzed using a family of model atmospheres with different He/H ratios. Atmospheric parameters are estimated from the ionization equilibrium set by neutral and singly ionized species of Fe and Mg, the excitation of Fe I and Fe II lines, and the wings of the Paschen lines. On the assumption that the He I lines are of photospheric and not chromospheric origin, a He/H ratio of approximately unity is found by imposing the condition that the adopted He/H ratio of the model atmosphere must equal the ratio derived from the observed He I triplet lines at 5876, 4471 and 4713 Å, and singlet lines at 4922 and 5015 Å. Using the model with the best-fitting atmospheric parameters for this He/H ratio, SAO 40039 is confirmed to exhibit mild dust-gas depletion, i.e., the star has an atmosphere deficient in elements of high condensation temperature. The star appears to be moderately metal-deficient with $[\text{Fe}/\text{H}] = -0.4$ dex. But the star's intrinsic metallicity as estimated from Na, S and Zn, elements of a low condensation temperature, is $[\text{Fe}/\text{H}]_0^1 = \simeq -0.2$. The star is enriched in N and perhaps O too, changes reflecting the star's AGB past and the event that led to He enrichment.

Subject headings: stars: fundamental parameters— stars: atmospheres— stars: evolution— stars: abundances

²Indian Institute of Astrophysics, Bengaluru-560034, India;
sumangala@iiap.res.in; pandey@iiap.res.in; giridhar@iiap.res.in

³W. J. McDonald Observatory, The University of Texas, Austin, Texas, USA 78712;
dll@astro.as.utexas.edu

¹ $[\text{Fe}/\text{H}]_0$ refers to the star's intrinsic metallicity

1. Introduction

SAO 40039, also known as IRAS 05040+4820 and BD +48°1220, is judged by several criteria to be a post-AGB star: its spectral type (A4Ia), its position in the IRAS color-color diagram and the double-peaked spectral energy distribution indicating a detached youthful cold dust shell around the central star. Using VBRIJHK photometry and adopting a simple dust shell model, Fujii et al. (2002) find a dynamical age of 2460 years for the dust shell with dust at 97K, and estimate the star to have a core mass of $0.55M_{\odot}$ indicating a low-mass progenitor for this PAGB star.

Klochko et al. (2007) have presented an abundance analysis of SAO 40039 based on high-resolution spectra with a wavelength coverage of 4500-6760Å. They have also discussed the star’s radial velocity changes and also time-dependent differential velocity shifts between different classes of absorption lines. Their spectra showed a variable $H\alpha$ line with two emission components. Variable emission was also reported in $H\beta$ and in some lines of Si II, Fe I and Fe II. But, in particular, these authors pointed out the abnormal strength of the He I 5876Å absorption feature in this star with the ‘low’ effective temperature of about 8000 K. Their abundance analyses conducted with model atmospheres computed for a normal He/H ratio ($=0.1$) gave the He/H ratio of 0.7.

Detection of He I lines in absorption in several A and F-type PAGB stars has been reported previously. The 4471Å line was found by Waelkens et al. (1992) in HD 44179, the central star of the Red Rectangle. HD 187885, a PAGB star with a high C/O ratio and an enrichment of *s*-process elements, shows the He I 5876 Å line (Van Winckel et al. 1996). Klochko et al. (2002) report five He I lines in HD 331319. Detection of He I lines in A and F-type supergiants suggest either a He enrichment, if the lines are of photospheric origin, or a contribution from a thick hot chromosphere of presumably a normal He abundance. The above studies adopt the assumption of a photospheric origin and report the photosphere to be moderately H-poor and He-rich. However, these analyses use model atmospheres computed for a normal He/H ratio and do not iterate on the construction of the model atmosphere and the abundance analysis to obtain agreement between the input and output He/H ratio.

Our goal in making a fresh analysis of SAO 40039 is to iterate to find the self-consistent He/H ratio. In undertaking the analysis, we also adopt the assumption that the He I lines originate in a He-rich photosphere and are not chromospheric in origin.

2. Observations and data reduction

Spectra of SAO 40039 were obtained on the nights of 2007 November 5 and 2011 February 21 at the W.J. McDonald Observatory with the 2.7m Harlan J. Smith telescope and the Tull coude spectrograph (Tull et al. 1995). The spectra taken at these epochs were found to be similar. The spectra correspond to a resolving power of 60,000 (5 kms s^{-1}). Reduction of the raw data was performed with the Image Reduction and Analysis Facility (IRAF²) software package.

An additional spectrum was obtained on 2011 January 28 using the echelle spectrometer at Vainu Bappu Observatory in Kavalur, India giving a resolution of about 28,000 (10 kms s^{-1}) in slitless mode (Rao et al. 2005). **Since the projected rotational velocity of the star is about 15 kms s^{-1} , the lower resolution of the VBO spectrum does not affect the stellar absorption profiles and hence our measured equivalent widths and the calculated abundances.**

3. Abundance Analysis

Our spectra resemble closely those described by Klochkova et al. (2007) with regards to emission in Balmer lines, the complex structure of the Na D lines and variable profiles of the metallic lines, and the equivalent widths of lines unaffected by obvious emission. For our analysis we have used only clean, unblended and symmetric absorption lines.

We have compared the equivalent widths of lines common between our spectra and those of Klochkova et al. (2007). A small systematic difference possibly caused by differences in resolution is discernible, but it appears that there were no major variations in the atmospheric parameters at these epochs. This is also supported by the fact that the average radial velocity of lines in our spectra (-12 kms s^{-1}) lies within the range as reported by Klochkova et al. (2007) in their spectra (-7 to -15 kms s^{-1}).

Abundance analysis was done first on the assumption that the atmosphere has a normal He/H ratio. Model atmospheres for normal He/H ratio (He/H=0.1) were taken from the Kurucz database³. Atmospheres of different He/H ratios were computed by the code STERNE (Jeffery et al. 2001). The LTE spectrum synthesis code MOOG (2009 version) by Sneden

²The IRAF software is distributed by the National Optical Astronomy Observatories under contract with the National Science Foundation

³<http://kurucz.harvard.edu/grids.html>

(1974) was used with the grid of model atmospheres taken from the Kurucz database as mentioned above. The LTE code SPECTRUM (Jeffery et al. 2001) was used with the STERNE models.⁴

The procedure begins with the determination of the atmospheric parameters from the spectrum, continues with the abundance analysis for He and other elements and ends when the model of a certain He/H ratio reproduces the observed He I lines.

3.1. Method for determining the stellar parameters

First, we estimated the microturbulent velocity (ξ_t) using Fe II lines with small range in lower excitation potentials (LEP)(2.6–3.2 eV) as these lines have a good range in their equivalent widths thereby reducing any temperature dependence of the estimated ξ_t . The ξ_t is found from the standard requirement that the abundance be independent of the measured equivalent width. The effective temperature (T_{eff}) was estimated by the requirement that the abundance of a given species be independent of a line’s LEP. This step was conducted independently for Fe I and Fe II lines as they are both well represented in the spectrum and show a range in their LEP’s. Finally, the surface gravity ($\log g$) was estimated by the condition that there be ionization balance between the neutral and the singly ionized Fe lines. This condition defines a locus in the (T_{eff} , $\log g$) plane and the T_{eff} derived from Fe I and Fe II breaks the degeneracy. This exercise is repeated for grids of model atmospheres with He:H ratios of 10:90, 30:70 and 50:50.

A microturbulence $\xi_t = 4.8 \pm 1.0 \text{ km s}^{-1}$ is found for all models with acceptable effective temperature and surface gravity and the value is insensitive to the He/H ratio of the models. The effective temperature T_{eff} is found to be $8000 \pm 300 \text{ K}$ from 26 Fe I and 20 Fe II lines. Within the 300K uncertainty, the temperature is independent of surface gravity over a considerable range and is not sensitive to the He/H ratio of the model atmosphere.

The T_{eff} , $\log g$ locus found from the ionization balance for Fe is illustrated in Figure 1 for the model atmosphere grid with He:H = 50:50. With $T_{\text{eff}} = 8000 \pm 300 \text{ K}$ from the excitation of Fe I and Fe II, the $\log g = 0.75 \pm 0.25 \text{ cgs}$ is found. The surface gravity changes slightly with He:H running from 0.94 for He:H=10:90 through 0.83 for He:H=30:70 to the above result for He:H=50:50. A second locus is provided by Mg I and Mg II lines – see upper

⁴Note that the stellar parameters and the abundances derived by adopting the Kurucz models and the code MOOG for He/H = 0.1 are in excellent agreement with results from the STERNE models and the LTE code SPECTRUM, also for He/H = 0.1.

panel of Figure 1. The Mg and Fe loci are in good agreement. A third locus is offered by the Paschen lines (see below).

3.2. The He/H ratio

Our spectra confirm the presence of the D3 5876Å He I line with an equivalent width very similar to that reported by Klochkova et al. (2007). The strength of this line suggests that several other lines should be present unless the excitation of the D3 line is highly peculiar. Our search also provided the additional triplets (4471 and 4713Å) and two singlet lines (4921 and 5015Å). Since the He I at 4713Å is blended with the Fe II line, its contribution has been included while synthesizing the He I profile at 4713Å as shown in the Figure 2, we get a consistent He/H ratio of approximately unity. Other possible He I lines are predicted to be below the detection limit, or blended with other lines or inaccessible due to inter-order gaps.

The He I lines were computed for model atmospheres with $(T_{\text{eff}}, \log g, \xi_t) = (8000, 0.75, 4.8)$ and with the appropriate model for the He/H ratios: 0.1 (normal; solar abundance), 0.4 (30/70), and 1.0 (50/50). The synthesized profiles are convolved with the instrumental and the stellar rotation profiles, before matching with the observed spectrum as described in Pandey (2006). The data for computing the He I profiles were taken from Jeffery et al. (2001). A projected rotational velocity of about 13–16 km s⁻¹ is estimated by using unblended moderately strong lines. As shown in Figure 2, the best fits to the observed He I profiles at 5875, 4471, 4713, 4922 and 5015Å were obtained for He/H ratio of 1.0 (50/50) with an uncertainty of approximately ± 0.2 .

To verify the model atmosphere parameters, we explore fits to the Paschen lines. The Balmer lines are affected by emission and blends with other lines for their line profiles to be useful as monitors of the atmospheric parameters but the Paschen lines appear free of emission and blends. The Stark broadening tables for the Paschen lines of hydrogen are taken from Lemke (1997). In the lower panel of the Figure 1, we show observed and synthesized Paschen profiles near 8600Å for the model with He/H=1.0 and $T_{\text{eff}} = 8000\text{K}$ and for surface gravities $\log g = 0.5, 0.75$ and 1.0. The best fitting profile is for $\log g$ of 0.75. We also synthesized the Paschen lines in the 8400Å region for the above mentioned temperature and gravities and we get consistent results. These profiles are also sensitive to the adopted effective temperature with a 1000K increase approximately mimicking a 0.5 dex increase in surface gravity. The Paschen lines give the locus shown in the upper panel of Figure 1. As the Paschen limit is approached, the Paschen lines overlap and depress the local continuum. In addition, the location of the continuum is rendered more challenging because of the echelle’s blaze function. Yet, the synthesized profiles closer to the limit are able to reproduce the

observed profiles quite well – see lower panel of Figure 1.

Our demonstration that SAO 40039 is H-deficient and He-rich rests on the assumption that the He I absorption lines originate in the stellar photosphere and are not a product of a stellar chromosphere. (A second assumption is that the real stellar photosphere approximates the model atmospheres computed by classical procedures). A chromospheric origin is not trivially dismissed. One recalls that the D3 line appears in absorption in spectra of F dwarfs with active chromospheres (Wolff & Heasley 1984; Danks & Lambert 1985); the correlation between D3 equivalent width and X-ray luminosity points strongly to a chromospheric origin. A chromospheric origin for He absorption is required to account for the presence of He I 10830 Å in spectra of warm-cool giants and supergiants where it may appear in absorption and/or emission (O’Brien & Lambert 1986) and cannot be of photospheric origin.

The possibility of the photospheric origin of the He I lines in our spectrum is supported by several facts. Firstly, the lines have the photospheric velocity. Secondly and more importantly, the equivalent widths of all He I lines – singlets and triplets – are reproduced by a photospheric model. If the lines originated in the chromosphere, one would expect a difference between singlets and triplets, as previously noted by Klochkova et al. (2002) in their discussion of the He I absorption lines found in HD 331319, a star similar to SAO 40039. While our analysis do not preclude a chromospheric origin, we agree with Klochkova et al. who remark ‘the hypothesis of a photospheric origin for the He I lines in HD 331319 is not rejected’. Certainly, there must be a suspicion that SAO 40039’s atmosphere is mildly H-deficient such that He/H = 1 now, a value indicating appreciable loss of H and enrichment of He since the star was a main sequence star with He/H \simeq 0.1.

4. Discussion and Results

Using the adopted model parameters (T_{eff} , $\log g$, ξ_t)=(8000, 0.75, 4.8) with He/H of 1.0, the measured equivalent widths of different species were used to derive the abundances. In Table 1 we present the abundances derived with the SPECTRUM code using the He/H=1.0 model and the abundances generated with the code MOOG using the He/H=0.1 model.

A detailed line list (see for SAMPLE Table 2, that lists some lines of SAO 40039) used in our analysis has been presented electronically. The line list provides the lower excitation potential (χ) for each line, the $\log gf$ value, sources of $\log gf$, the measured equivalent widths (W_λ) in mÅ, the abundance ($\log \epsilon$) derived from each line for the adopted model atmosphere.

The solar abundances for all the elements have been taken from Asplund et al. (2009).

SAO 40039 seems to be mildly iron-poor. Klochkova et al.’s analysis assuming $\text{He}/\text{H}=0.1$ gave a solar Fe abundance, a value essentially confirmed by our analysis for the model atmosphere also with $\text{He}/\text{H} = 0.1$. A principal effect of the higher He abundance is to reduce the continuous opacity per gram and so demand a lower iron abundance to match the same observed line strength. Inspection of the $[\text{X}/\text{Fe}]$ entries in Table 1 points to several anomalies when the composition of an unevolved disk star is taken as the reference. The two most extreme anomalies are nitrogen which is very overabundant ($[\text{N}/\text{Fe}] = +1.1$), and aluminium which is markedly under-abundant ($[\text{Al}/\text{Fe}] = -0.7$). Closer study shows that sodium may be overabundant ($[\text{Na}/\text{Fe}] = +0.3$) and a suite of elements are mildly under-abundant: Ca, Sc, Ti, Zr and Ba with $[\text{El}/\text{Fe}] \simeq -0.35$.

This abundance pattern is largely reminiscent of the pattern exhibited by stars affected by dust-gas separation, i.e., the photosphere is dominated by accretion of gas but not dust from a cool envelope, possibly a circumbinary dusty disk. Dust-gas separation is most remarkably exhibited by post-AGB binaries such as HR 4049 (Van Winckel 2003). In such cases, the abundance anomalies are correlated with the condensation temperature (T_c): elements with high T_c are most under-abundant. In Figure 3, we plot $[\text{X}]$ (where $[\text{X}] = \log \epsilon(\text{X})_* - \log \epsilon(\text{X})_\odot$) versus the T_c computed by Lodders (2003) for a solar composition mixture. Elements N and O depart from a general tendency for $[\text{X}]$ to decrease with increasing T_c . In presenting Figure 3, the adopted reference has been that $[\text{X}/\text{Fe}] \simeq 0.0$ for all elements in an unevolved star with $[\text{Fe}/\text{H}] \simeq -0.4$. This is essentially true for a thin disk star, although a dispersion in heavy elements at a given $[\text{Fe}/\text{H}]$ was noted by Edvardsson et al. (1993). If SAO 40039 is a thick disk star, the α -elements in Figure 3 should be plotted with $[\text{X}]$ about -0.2 dex less than shown in the figure but the overall trend and the scatter about that trend will be unaffected. The Na, S, and Zn abundances suggest that the initial metallicity of the star was $[\text{Fe}/\text{H}]_0 \simeq -0.2$.

The high N abundance is, probably, a consequence of extensive burning of H to He by the CN-cycle with concomitant conversion of C to N. Survival of C at about its initial abundance suggests that N synthesis occurred primarily after the atmosphere was enriched with C at the third dredge-up. One possibility is H-consumption during a final He-shell flash (Herwig 2001; Bloeker 2001). The O is overabundant with respect to the initial abundance, possibly it was enriched by the third dredge-up and temperatures during the late episode of H-burning were too low to destroy O or non-LTE line formation can reduce the C, N and O abundances. For an effective temperature of about 8000K, Venn (1995) give non-LTE correction to C and N abundances from C I and N I lines of about -0.4 dex for normal supergiants. Takeda & Takada-Hidai (1998) have estimated NLTE corrections for O I to be -0.1 dex at this effective temperature for supergiants. After applying these non-LTE corrections, the above sketch of a possible origin for SAO 40039 is little affected.

5. Concluding remarks

Though, the existence of extremely H-deficient stars with He/H ratio of about 10,000, showing He I lines in their absorption spectra, is known (Pandey et al. 2001; Pandey & Reddy 2006), SAO 40039, from our estimated He/H ratio of about unity, appears to be the first detection of a mildly H-deficient star. Lambert (1996) had commented on the possibilities of such stars and on the difficulty in detection for stars too cool to show He I lines. With an effective temperature of about 8000K, SAO 40039 seems to be responding to this call.

It is very likely that other post-AGB stars may belong to the mildly H-deficient class. Several examples like SAO 40039 have detectable He I lines. The question then arises; are post-AGB stars of a temperature too low to provide He I lines also He-rich and how can their H-deficiency be unmasked? Exploration of post-AGB stars showing He I lines need to be continued with models of appropriate H/He ratios. Additionally, non-LTE abundance analyses as described by Pandey & Lambert (2011) should be performed to further refine knowledge of the chemical compositions.

We are thankful to the VBO observing support team, in particular to Mr G. Selvakumar, for obtaining a spectrum of SAO 40039 using the VBT echelle spectrometer. DLL thanks the Robert A. Welch Foundation of Houston, Texas for support through grant F-634.

REFERENCES

- Asplund, M., Grevesse, N., Sauval, A. J., & Scott, P., 2009, *ARA&A*, 47, 481
- Blöcker, T., 2001, *Ap&SS*, 275, 1
- Danks, A. C., & Lambert, D. L., 1985, *A&A*, 148, 293
- Edvardsson, B., Andersen, J., Gustafsson, B., Lambert, D. L., Nissen, P. E., & Tomkin, J., 1993, *A&A*, 275, 101
- Fujii, T., Nakada, Y., & Parthasarathy, M., 2002, *A&A*, 385, 884
- Herwig, F., 2001, *Ap&SS*, 275, 15
- Jeffery, C. S., Woolf, V. M., & Pollacco, D. L. 2001, *A&A*, 376, 497
- Klochkova, V. G., Chentsov, E. L., Tavalzhanskaya, N. S., & Panchuk, V. E., 2007, *Astronomy Reports*, 51, 642
- Klochkova, V. G., Panchuk, V. E., & Tavalzhanskaya, N. S., 2002, *Astronomy Letters*, 28, 49
- Lambert, D. L., 1996, *ASP Conf. Ser.*, 96, 443
- Lemke, M., 1997, *A&AS*, 122, 285
- Lodders, K., 2003, *ApJ*, 591, 1220
- O’Brien, G. T. Jr., & Lambert, D. L., 1986, *ApJS*, 62, 899
- Pandey, G., Rao, N. K., Lambert, D. L., Jeffery, C. S., & Asplund, M. 2001, *MNRAS*, 324, 937
- Pandey, G. 2006, *ApJ*, 648, L143
- Pandey, G., & Reddy, B. E., 2006, *MNRAS*, 369, 1677
- Pandey, G., & Lambert, D. L., 2011, *ApJ*, 727, 122
- Rao, N. K., Sriram, S., Jayakumar, K., & Gabriel, F., 2005, *JA&A*, 26, 331
- Snedden, C., 1973, Ph.D Thesis, Univ. of Texas at Austin, USA
- Takeda, Y., & Takada-Hidai, M., 1998, *PASJ*, 50, 629

- Tull, R. G., MacQueen, P. J., Sneden, C., & Lambert, D. L., 1995, *PASP*, 107, 251
- Van Winckel, H., Waelkens, C., & Waters, L. B. F. M., 1996, *A&A*, 306, L37
- Van Winckel, H., 2003, *ARA&A*, 41, 391
- Venn, K. A., 1995, *ApJ*, 449, 839
- Waelkens, C., Van Winckel, H., Trams, N. R., & Waters, L. B. F. M., 1992, *A&A*, 256, L15
- Wolff, S. C., & Heasley, J. N., 1984, *PASP*, 96, 231

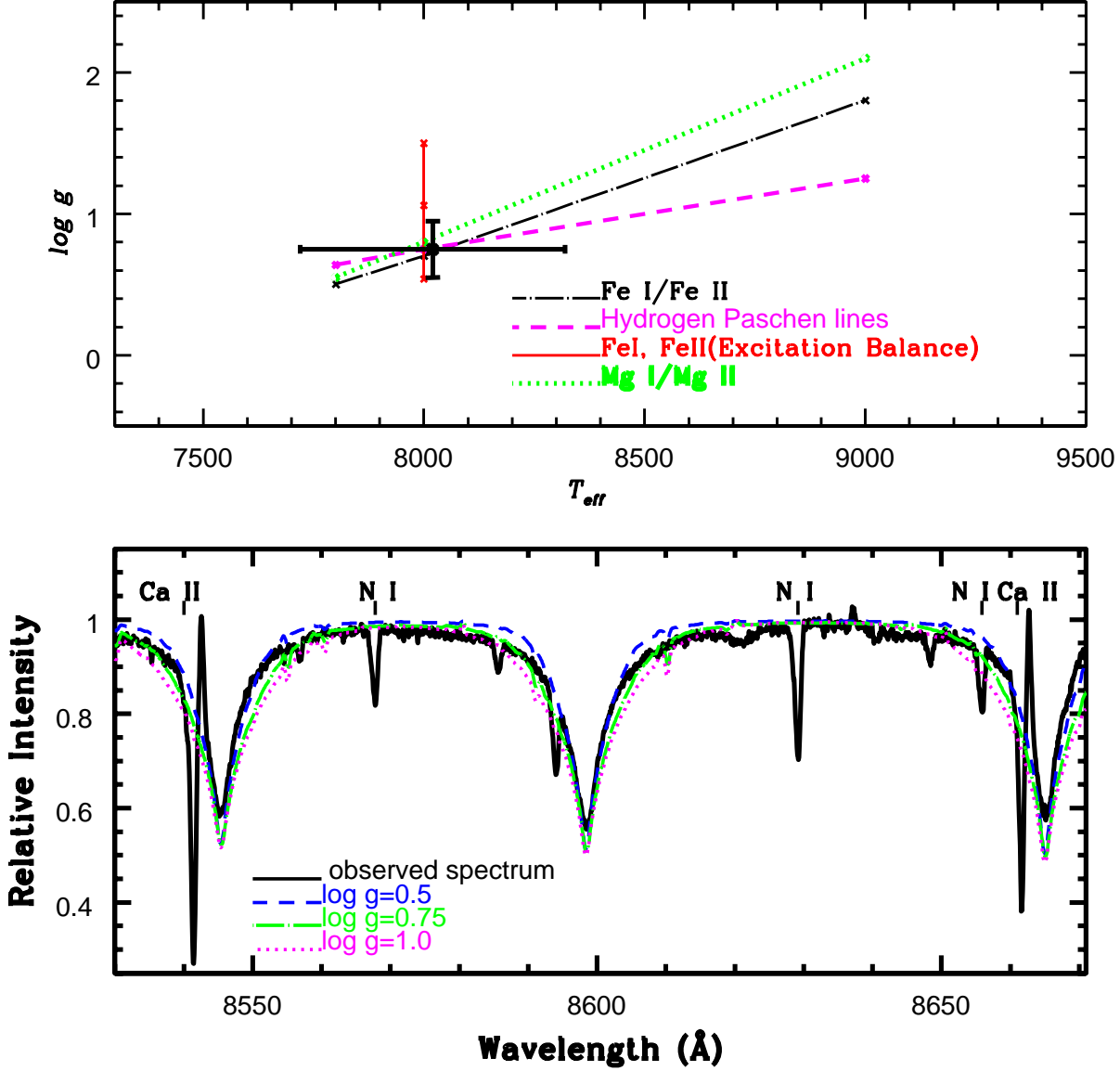


Fig. 1.— The upper panel shows the loci satisfying the ionization balance — see keys on the figure. The locus satisfying the H I Paschen lines is shown by dashed line. The solid line represents the excitation balance of both Fe I and Fe II. The cross shows the derived stellar parameters. Lower Panel shows the observed and synthesized profiles of Paschen lines of H I in the 8600Å region for $T_{\text{eff}} = 8000\text{K}$, $\text{He}/\text{H} = 1.0$ and $\log g = 0.5, 0.75$ and 1.0 — see keys on the figure.

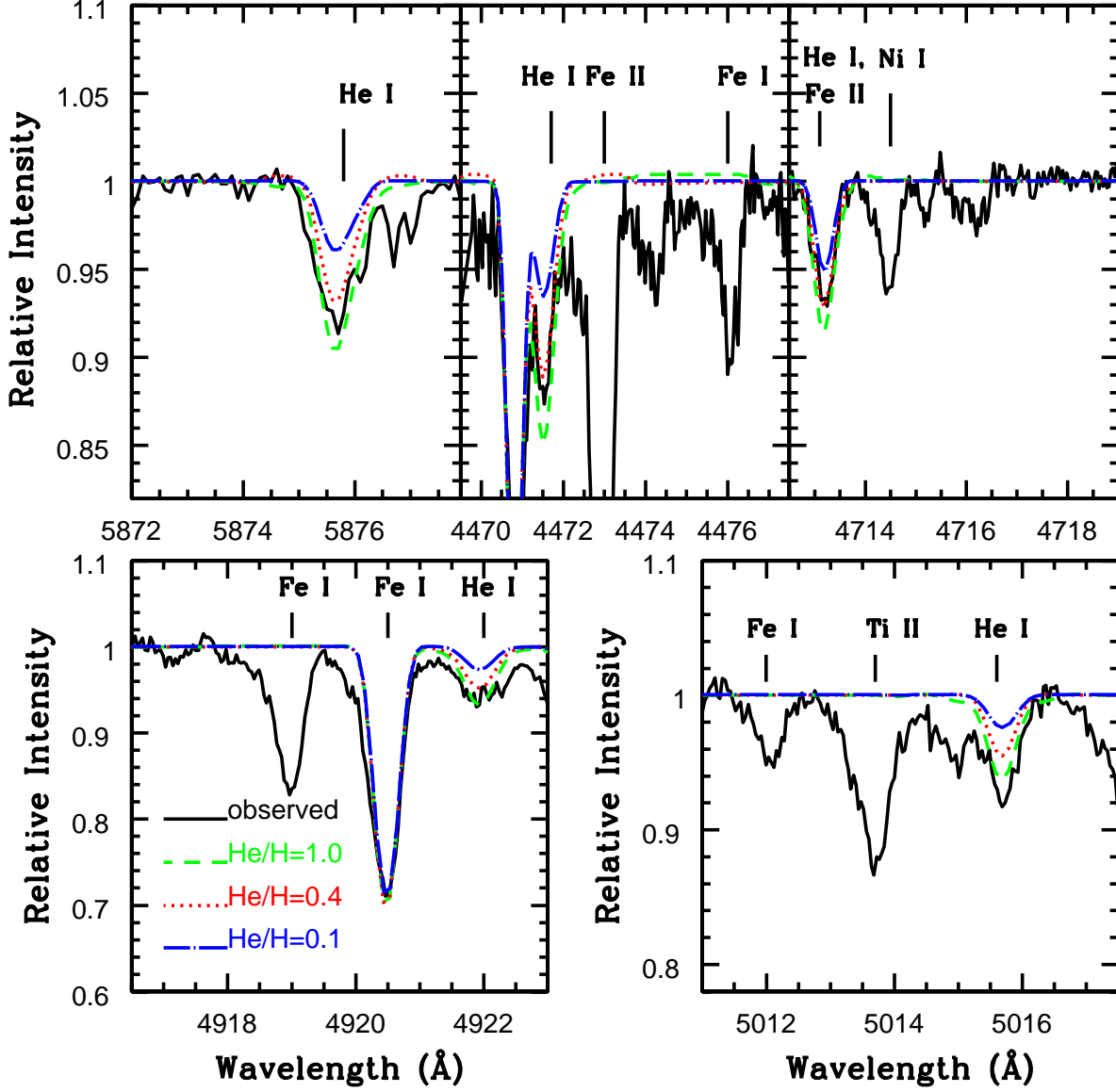


Fig. 2.— The observed and synthesized He I profiles for the triplet lines at 5876, 4471 and 4713Å and for the singlet lines at 4922 and 5015Å for SAO 40039 using models with $T_{\text{eff}} = 8000\text{K}$, $\log g = 0.75$ for $\text{He}/\text{H} = 1.0, 0.4$ and 0.1 – see keys on the figure.

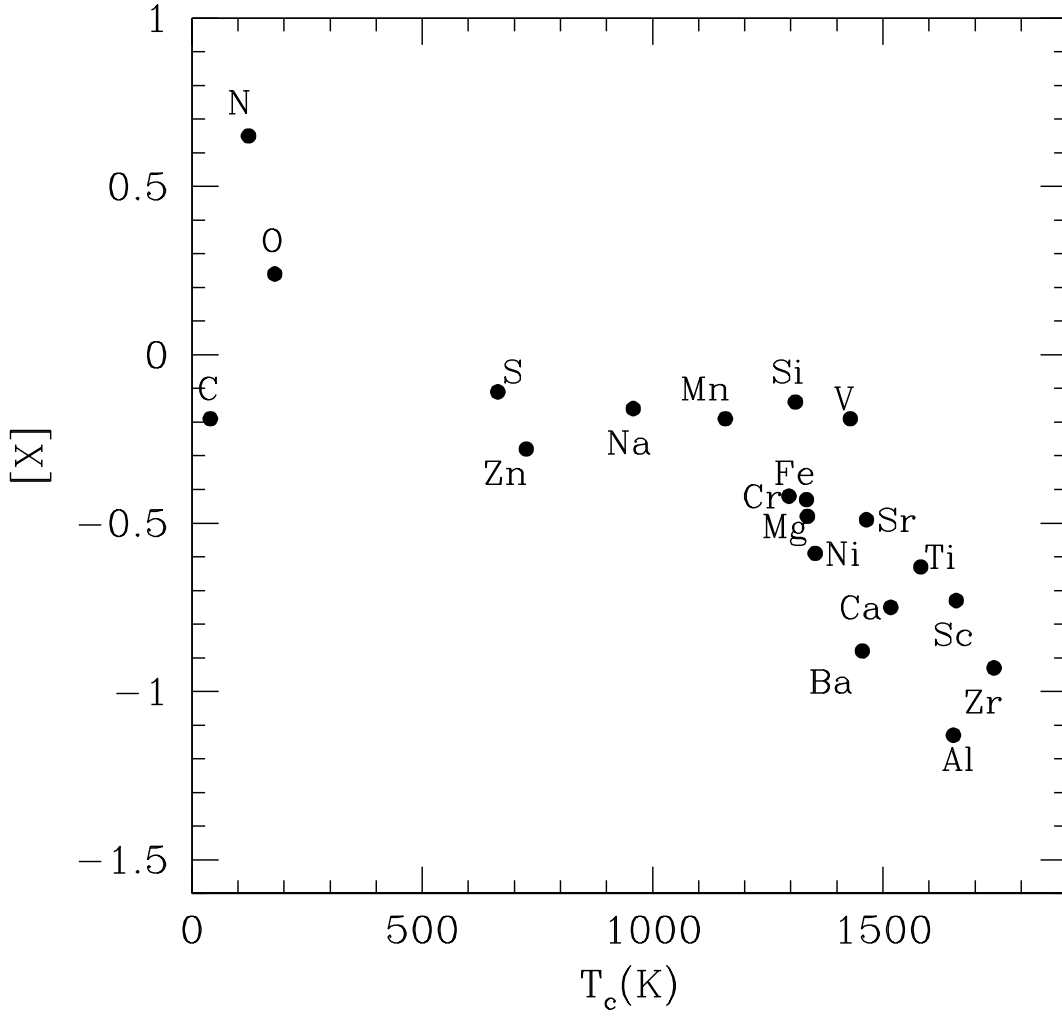


Fig. 3.— The $[X]$ versus T_c plot for SAO 40039.

Table 1. Comparison between abundances estimated with MOOG using He/H=0.1 model and the abundances computed with SPECTRUM using the hydrogen deficient (He/H=1.0) model

Species	MOOG ^a				SPECTRUM ^b				SPECTRUM ^c	
	$\log \epsilon_{\odot}$	$\log \epsilon$	[X/Fe]	n	$\log \epsilon$	[X/Fe]	n	Δ^d	[X/Fe]	n
H I	12.00	12.00	11.45
He I	10.98	10.98	11.45	0.2
Li I	3.26	4.03	$<+0.68\pm0.00$	1	3.50	$<+0.67\pm0.00$	1
C I	8.43	8.78	$+0.26\pm0.16$	21	8.24	$+0.24\pm0.16$	21	0.3	$+0.27\pm0.18$	9
N I	7.83	9.05	$+1.13\pm0.25$	9	8.48	$+1.08\pm0.20$	9	0.1	$+1.32\pm0.04$	2
O I	8.69	9.47	$+0.69\pm0.15$	8	8.93	$+0.67\pm0.14$	8	0.1	$+0.76\pm0.14$	2
Na I	6.24	6.58	$+0.25\pm0.10$	2	6.08	$+0.27\pm0.07$	2	0.3
Mg I	7.60	7.76	$+0.07\pm0.31$	4	7.13	-0.04 ± 0.18	4	0.4	-0.26 ± 0.11	2
Mg II	7.60	7.78	$+0.09\pm0.15$	4	7.12	-0.05 ± 0.15	4	0.1	-0.10 ± 0.03	3
Al I	6.45	5.95	-0.59 ± 0.01	2	5.32	-0.70 ± 0.03	2	0.4
Si II	7.51	7.90	$+0.30\pm0.16$	3	7.37	$+0.29\pm0.13$	3	0.2	$+0.31\pm0.00$	1
S I	7.12	7.53	$+0.32\pm0.01$	2	7.01	$+0.32\pm0.02$	2	0.3
Ca I	6.34	6.18	-0.25 ± 0.12	2	5.55	-0.36 ± 0.16	2
Ca II	6.34	6.21	-0.22 ± 0.00	1	5.64	-0.27 ± 0.00	1	0.4	-0.36 ± 0.00	1
Sc II	3.15	2.89	-0.35 ± 0.17	5	2.42	-0.30 ± 0.15	5	0.3	-0.05 ± 0.16	2
Ti II	4.95	4.83	-0.21 ± 0.23	20	4.32	-0.20 ± 0.20	20	0.3	-0.24 ± 0.16	12
V II	3.93	4.21	$+0.19\pm0.04$	2	3.74	$+0.24\pm0.03$	2	0.2
Cr I	5.64	5.62	-0.11 ± 0.13	3	5.11	-0.10 ± 0.10	3	0.4	-0.06 ± 0.23	2
Cr II	5.64	5.83	$+0.10\pm0.11$	9	5.33	$+0.12\pm0.10$	9	0.2	$+0.09\pm0.06$	4
Mn II	5.43	5.73	$+0.21\pm0.00$	1	5.24	$+0.24\pm0.00$	1
Fe I	7.50	7.54	-0.05 ± 0.18	26	7.02	-0.05 ± 0.17	26	0.4	-0.01 ± 0.19	7
Fe II	7.50	7.65	$+0.06\pm0.19$	20	7.13	$+0.06\pm0.17$	20	0.2	$+0.01\pm0.14$	9
Ni I	6.22	6.16	-0.15 ± 0.15	4	5.63	-0.16 ± 0.14	4	0.3
Zn I	4.56	4.81	$+0.16\pm0.30$	2	4.28	$+0.15\pm0.23$	2	0.4
Sr II	2.87	3.01	$+0.05\pm0.07$	2	2.38	-0.06 ± 0.03	2
Zr II	2.58	2.13	-0.54 ± 0.08	2	1.65	-0.50 ± 0.04	2	0.3
Ba II	2.18	1.85	-0.42 ± 0.15	2	1.30	-0.45 ± 0.11	2	...	-0.35 ± 0.00	1
Eu II	0.52	0.40	$<-0.10\pm0.00$	1	0.15	$<+0.06\pm0.00$	1

^aMOOG abundances computed using the He/H=0.1 model for the McDonald spectra.

^bSPECTRUM abundances computed using the He/H=1.0 model for the McDonald spectra.

^cSPECTRUM abundances computed using the He/H=1.0 model for the VBO spectra.

^d Δ corresponds to the square root of the sum of the squares of the abundance errors due to uncertainties in the stellar parameters: ΔT_{eff} , $\Delta \log g$ and $\Delta \xi_t$

Table 2. Detailed line list for SAO 40039¹

Line	χ (eV)	$\log gf$	W_λ (mÅ)	$\log \epsilon$
He I λ 5875.61	20.96	+0.739 ^a	Synth	11.45
He I λ 4471.47	20.96	+0.053 ^a	Synth	11.40
He I λ 4921.93	21.21	−0.435 ^a	Synth	11.45
He I λ 5015.67	20.61	−0.819 ^a	Synth	11.50
He I λ 4713.13	20.96	−0.975 ^a	Synth	11.40
C I λ 4775.87	7.49	−2.304 ^a	35	8.41
C I λ 5039.05	7.48	−2.100 ^a	33	8.15
C I λ 4770.02	7.48	−2.437 ^a	30	8.45
C I λ 4766.67	7.48	−2.400 ^a	26	8.34
C I λ 4826.80	7.49	−2.140 ^a	24	8.04

^aNIST database (http://physics.nist.gov/PhysRefData/ASD/lines_form.html)

¹Table 2 is published in its entirety in the electronic edition of ApJ. A portion is shown here for guidance regarding its form and content.